Remote Sensing of Environment 114 (2010) 1710–1717

Contents lists available at ScienceDirect

Remote Sensing of Environment

journal homepage: www.elsevier.com/locate/rse

The effects of rectification and Global Positioning System errors on satellite image-based estimates of forest area

Ronald E. McRoberts

Northern Research Station, U.S. Forest Service, Saint Paul, MN, USA

ARTICLE INFO

Article history:
Received 20 November 2009
Received in revised form 17 February 2010
Accepted 3 March 2010

Keywords:
Logistic regression
Inference
Forest inventory

ABSTRACT

Satellite image-based maps of forest attributes are of considerable interest and are used for multiple purposes such as international reporting by countries that have no national forest inventory and small area estimation for all countries. Construction of the maps typically entails, in part, rectifying the satellite images to a geographic coordinate system, observing ground plots whose coordinates are obtained from Global Positioning System (GPS) receivers that are calibrated to the same geographic coordinate system, and then matching ground plots to image pixels containing the centers of the ground plots. Errors in rectification and GPS coordinates cause observations of ground attributes to be associated with spectral values of incorrect pixels which, in turn, introduces classification errors into the resulting maps. The most important finding of the study is that for common magnitudes of rectification and GPS errors, as many as half the ground plots may be assigned to incorrect pixels. The effects on areal estimates obtained by aggregating class predictions for individual pixels are deviation of the estimates from their true values, erroneous confidence intervals, and incorrect inferences. Results are reported in detail for both probability-based (design-based) and model-based approaches to inference for proportion forest area using maps constructed from Landsat imagery, forest inventory plot observations and a logistic regression model.

Published by Elsevier Inc.

1. Introduction

Forest area is an indicator specified by the two primary forest sustainability agreements, the Montréal Process (2005) and the Ministerial Convention on the Protection of Forests in Europe (2009). In addition, parties to the United Nations Framework Convention on Climate Change (UNFCCC, 2007) and the Kyoto Protocol (1997) submit annual reports of carbon emissions for six land use categories of which one is forest. Of particular note in the context of climate change, forest is the only land cover category whose resources can be managed to produce a positive effect on the greenhouse gas balance (Cienciala et al., 2008). At the invitation of the seventh conference of parties to the UNFCCC, known as COP-7, the Intergovernmental Panel on Climate Change prepared and adopted good practice guidelines (GPG) for the Land-Use, Land-Use Change, Forests (LULUCF) sector. The GPG assist countries in conducting forest inventories for the LULUCF sector with emphasis on issues related to assessing, managing, and reducing bias and uncertainty.

The primary sources of information used to estimate forest area for large areas are the national forest inventories (NFI) conducted by countries in North America, Europe, Asia and elsewhere. Tomppo et al. (2010) provide a survey of NFIs and their approaches to estimating forest attributes. For countries that lack or are just initiating NFIs, particularly in tropical areas where forest land is less accessible, estimates of forest area are often based on classifications of medium resolution, multi-spectral satellite imagery such as Landsat or SPOT. In many countries with NFIs, users frequently request estimates for small areas for which NFI sample sizes are too small to produce acceptably precise estimates, and they frequently request map products consistent with the estimates. Often the solution to small area estimation is also satellite image-based maps of forest attributes. Thus, because of their wide-spread use, all issues related to satellite image-based maps of forest area warrant assessment.

Construction of forest attribute maps using satellite imagery typically requires reference data in the form of ground observations, although interpretations of aerial photography are often used as surrogates for ground observations. Two crucial tasks are necessary to construct spatially accurate maps: first, the satellite imagery must be rectified to a geographical coordinate system using ground control points whose coordinates are known and that can be readily identified on the imagery, and second, the locations of the reference observations in the same geographical coordinate system must be determined. The latter task is usually accomplished using Global Positioning System (GPS) receivers that have been calibrated to produce coordinates in the same system as the one to which the imagery has been rectified. Following accomplishment of these two tasks, the relationship between the land cover classes of the reference observations and the image spectral data is estimated, and the land cover class for each image pixel is predicted.

E-mail address: rmcroberts@fs.fed.us.

0034-4257/$ – see front matter. Published by Elsevier Inc.
doi:10.1016/j.rse.2010.03.001

The most commonly assessed errors in maps are characterized as classification or thematic errors. However, the effects of positional errors, which includes both rectification errors and GPS errors, on classification accuracy and inferences based on classifications are often ignored. As the label suggests, rectification error results from imperfect rectification of imagery to the coordinate system. Congalton (2007) asserts that topography is the primary factor affecting rectification accuracy and that rectification accuracy is an integral component of classification accuracy. Rectification error is typically quantified as the root mean square distance between known ground point locations and their locations in the rectified imagery. Congalton (2007) further indicates that rectification errors on order of a half-pixel width are sufficiently small for most applications using Landsat or SPOT imagery. Cooke (2000) and Patterson and Williams (2003), however, indicate that rectification error is typically as great as one pixel width, whereas Goodchild (1994) suggests that the pixels in which points appear in a map may be as many as two pixels away from the actual point location and may be anywhere within a 3×3 pixel array. Carmel et al. (2001) note that few studies have explored the combined effects of positional and classification error. Of the few, Arbia et al. (1998) found that rectification error had large effects on a wide range of map parameters.

In recent years, geographical coordinates of reference data used for image classification are typically acquired using GPS receivers. GPSs are based on the concept of triangulation whereby the coordinates of a point in three dimensions can be estimated from its distances to three points whose coordinates are known. For a GPS, the point whose coordinates are to be determined is the location of the GPS receiver, and the known points are satellites orbiting the earth. Distances are estimated from the elapsed time a signal emitted by a satellite and traveling at the speed of light takes to travel to the GPS receiver. The accuracy of the estimated coordinates of the receiver location depends on the method used to estimate the elapsed time. One method is based on a unique, pseudo-random code imposed on a carrier frequency emitted by each satellite. Both the satellite and the receiver use very accurate, synchronized clocks to generate this same pseudo-random code at exactly the same time. However, upon reaching the GPS receiver, the code will be slightly out of synchronization because of the time elapsed since its emission by the satellite. The time adjustment necessary to bring the two pseudo-random codes back into synchronization is the basis for estimating the elapsed time. Because of the relatively large cycles of the pseudo-random code, synchronization errors may occur with these code-phase GPS receivers and lead to positional errors of 1–100 m. A second and more accurate method is to synchronize the phases of the carrier frequency. Because the cycles are smaller, greater accuracy is possible. However, whereas the pseudo-random code is intentionally complex to facilitate synchronization, the carrier frequency is very uniform. Thus, with carrier-phase GPS receivers, the estimate of elapsed time is first approximated by synchronizing the pseudo-random code and is then refined by synchronizing the carrier phase. The result is better estimates of elapsed time and greater positional accuracy, often in the range 10–30 cm.

The Forest Inventory and Analysis (FIA) program of the U.S. Forest Service uses code-phase GPS receivers in the conduct of the NFI of the United States of America (USA). Cooke (2000) indicates that positional errors for these receivers are in the range 5–20 m, while Jasumback (1996) indicates that such errors have a mean of approximately 8 m and a maximum of 20 m. Riemann et al. (2000) and Hoppus et al. (2001) reported that 30% of classification errors for Landsat pixels could be attributed to errors between locations of ground reference and image data. Patterson and Williams (2003) found that plot location errors produced no detectable bias in post-stratified estimators of forest area, although estimated variances were too large with the effect of slightly increasing coverages for nominal 80% confidence intervals. McRoberts et al. (2002) found that errors in GPS locations of FIA plots had only a slight detrimental effect on the efficiency of stratified estimates of forest area.

When considering the combined effects of both rectification and GPS errors, Cooke (2000) suggested that in the worst case, the additive error may be approximately 50 m, whereas Czaplewski (2005) suggested that the combined error may be 0–70 m. Carmel et al. (2001) recommended quantifying the effects of positional error in terms of classification accuracy. Other than the studies reported by Arbia et al. (1998) and by scientists of the FIA program (Hoppus & Lister, 2007; Hoppus et al., 2001; McRoberts et al., 2002; Patterson & Williams, 2003; Riemann et al., 2000), few investigations have been reported of the effects of positional errors on classification accuracy or statistical inference for forest attributes. One exception is that numerous investigations over a considerable length of time have been reported of the detrimental effects of errors in registering two images to each other for purposes of change detection (Dai & Khorram, 1998; Magnussen, 2007; Pontius, 2000; Stow, 1999; Townshend et al., 1992).

Even fewer studies have been reported approaches for compensating for or correcting rectification and GPS errors. From the perspective of users of FIA data who co-register plots with spatial data from other sources, the preferred approach would be for field crews to use more accurate GPS receivers. The simplest approach to compensating for GPS errors would be to delete data for such plots if they can be correctly identified, if their spatial and thematic distributions can be assumed to be random, and if the adverse effects of degradation in sample sizes are tolerable. Four approaches to correcting errors have been suggested. Riemann et al. (2000) and Hoppus et al. (2001) investigated use of aerial photography to identify GPS errors which could then, perhaps, be corrected. They also investigated matching plot observations to the means of spectral values for 3×3 blocks of pixels. Halme and Tomppo (2001) reported a technique in which locations of field plots were re-assigned to Landsat pixels within a 7×7 pixel window using a weighted function of correlations among field and spectral values. The relocations produced reductions in root mean square errors for estimates of volume per unit area using the k-Nearest Neighbors technique of as much as 36%. Barber et al. (2006) proposed a Bayesian approach for which positional errors, quantified as differences between map and GPS locations, are estimated using a model-based approach, and map accuracy metadata are used as prior information.

In a broader context, a two-step approach to dealing with positional error merits consideration. The first step is to assess the effects of positional errors on selected measures such as classification accuracy or inferences based on the classifications. If the effects are sufficiently severe, where sufficiency is acknowledged to be subjective and dependent on the application, then a second step focusing on development of techniques for compensating for or correcting the errors is warranted. This study focuses on the first step and has as its objective the assessment of the effects of rectification and GPS errors on inferences for forest area using maps constructed using Landsat imagery, FIA plot data, and a logistic regression model.

2. Data

The study area was defined by the portion of the row 27, path 27, Landsat scene in northern Minnesota, USA (Fig. 1). Land use for the study area consists of forest land dominated by aspen–birch and spruce–fir associations, agriculture, wetlands, and water. Landsat Thematic Mapper (TM) imagery was acquired for three dates corresponding to early, peak, and late seasonal vegetative stages: April 2000, July 2001, and November 1999. Preliminary analyses indicated that the normalized difference vegetation index (NDVI) (Rouse et al., 1973) and the tasseled cap (TC) transformations (brightness, greenness, and wetness) (Crist & Cicone, 1984; Kauth & Thomas, 1976) were superior to both the spectral band data and principal component transformations with respect to predicting the

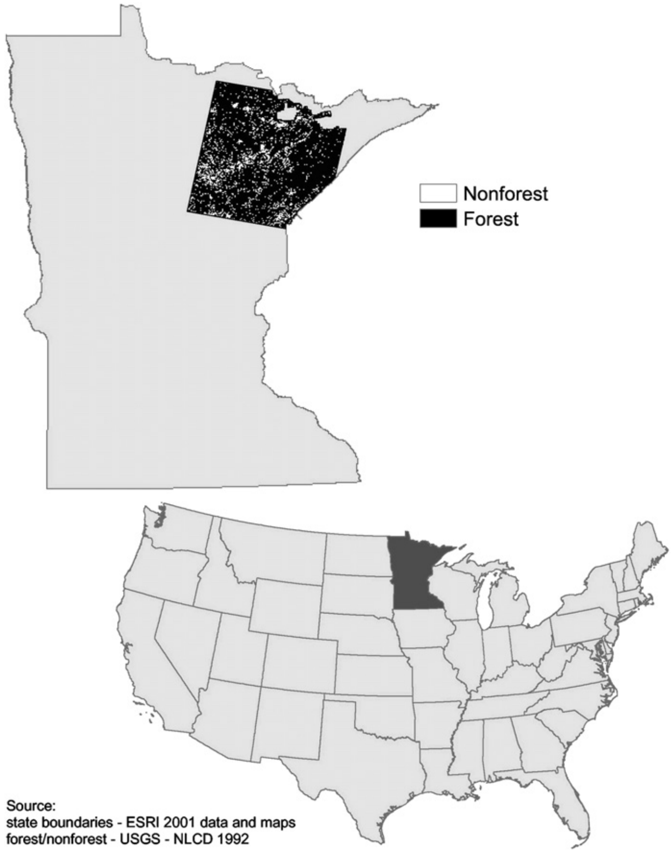

Fig. 1. Study area.

probability of land cover classes. Thus, 12 TM-based variables were used: NDVI and the three TC transformations for each of the three image dates. Within the study area, six 15-km × 15-km areas of interest (AOI) were selected using a systematic grid of locations.

The FIA program has established field plot centers in permanent locations using a sampling design that produces an equal probability sample (Bechtold & Patterson, 2005; McRoberts et al., 2005). The sampling design is based on a tessellation of the USA into approximate 2,400-ha (6,000-ac) hexagons and features a permanent plot at a randomly selected location within each hexagon. Some states, including Minnesota in which the study area is located, provide additional funding to double the sampling intensity to approximately one plot per 1200 ha.

Each FIA plot consists of four 7.32-m (24-ft) radius circular subplots that are configured as a central subplot and three peripheral subplots with centers located at 36.58 m (120 ft) and azimuths of 0°, 120°, and 240° from the center of the central subplot. In general, coordinates of the central subplots of forested or previously forested plots are determined using GPS receivers, whereas coordinates of central subplots of non-forested plots are verified using aerial imagery and digitization methods. Coordinates of the centers of peripheral subplots are calculated using their known azimuths and distances from the centers of the central subplots. For this study, only data for the central subplots of FIA plots were used because they are the only subplots whose coordinates are obtained using GPS receivers.

Forest area for each subplot is obtained by collapsing ground land use conditions into non-forest and multiple forest classes subject to the FIA definition of forest land: area of at least 0.4 ha (1 ac), continuous width of at least 36.58 m (120 ft), and stocking of at least 10% where stocking refers to the extent to which the growth potential of a site is used by trees (Hansen & Hahn, 1992). All plots were measured between 1999 and 2003. For this study, only completely forested or completely non-forested subplots of plots with centers in the six AOIs were used; of the 91 such subplots, 65 were completely forested and 26 were completely non-forested. The number of subplots per AOI ranged from 14 to 16.

3. Methods

All analyses were based on four underlying assumptions: (1) a finite population consisting of N units in the form of 30-m × 30-m Landsat pixels, (2) an equal probability sample of n population units in the form of forest/non-forest observations for the central subplots of FIA plots, (3) ancillary data in the form of the 12 Landsat-based spectral transformations for each population unit, and (4) adequate characterization of entire 900-m^2 pixels by the 167.87-m^2 subplots. In the sections that follow, the terms *population unit* and *pixel* are used interchangeably.

3.1. Logistic regression model

The forest/non-forest attribute may be considered a binomial variable: $y = 0$ for non-forest and $y = 1$ for forest. The relationship between a binomial dependent variable (e.g., forest/non-forest), Y, and continuous independent variables (e.g., image spectral transformations), $\mathbf{X}$, is often expressed in the form,

$$p_i = f(\mathbf{X}_i; \boldsymbol{\beta}),$$

where i indexes population units, p_i is the probability that $y_i = 1$ (forest), and $\boldsymbol{\beta}$ is a vector of parameters to be estimated (Agresti, 2007). The function, $f(\mathbf{X}_i;\boldsymbol{\beta})$, expresses the statistical expectation of Y in terms of $\mathbf{X}$ and $\boldsymbol{\beta}$ and is often formulated using the logistic function as,

$$p_i = f(X_i;\beta) = \frac{\exp\left(\sum_{j=1}^{J} \beta_j x_{ij}\right)}{1 + \exp\left(\sum_{j=1}^{J} \beta_j x_{ij}\right)}, \tag{1}$$

where $j = 1, 2, \ldots, J$ indexes the independent variables, and exp(.) is the exponential function.

3.2. Probability-based inference

Probability-based inference is based on three assumptions: (1) population units are selected for the sample using a randomization scheme; (2) the probability of selection for each population unit is positive and known; and (3) the observation of the response variable for each population unit is a constant as opposed to being a realization of a random variable. Properties of probability-based estimators are based on random variation resulting from the probabilities of selection of population units into the sample, thus the characterization of these estimators as probability-based (Hansen et al., 1978). Although probability-based inference is also characterized as design-based inference, the term *design* is not well-defined in the sense that it may refer simply to the selection of population units into the sample or additionally to the entire inferential process (Kendall & Buckland, 1982).

With probability-based methods, observations and predictions of land cover classes are both discrete values of a categorical variable. For areal assessments of maps, the objective is typically to estimate the total areas or the proportions of land cover classes. Because the estimate of the total area of a class is simply the product of total area which is usually known and an estimate of the class proportion, the focus of this study is estimation of the proportion. Probability-based approaches produce areal estimates, $\hat{\mu}$, of population parameters such as land cover class proportions using unbiased or nearly unbiased estimators, although an estimate based on any one sample may be far from the true value. For equal probability sampling designs such as that used by the FIA program, the simplest approach to probability-based areal inference for the proportion, μ, of an AOI in a particular land cover class is to use the familiar simple random sampling (SRS) estimators:

$$\hat{\mu}_{SRS} = \frac{1}{n}\sum_{i=1}^{n} y_i, \tag{2}$$

and,

$$\begin{aligned} V\hat{a}r(\hat{\mu}_{SRS}) &= \frac{\sum_{i=1}^{n}(y_i-\hat{\mu}_{SRS})^2}{n^2} \\ &= \frac{\hat{\mu}_{SRS}(1-\hat{\mu}_{SRS})}{n}, \end{aligned} \tag{3}$$

where i indexes the n sample observations, y_i is the observation for the ith population unit, and the subscript *SRS* denotes an estimator based on the assumption of simple random sampling. The advantages of SRS estimators are that they are intuitive, familiar, and simple; the disadvantages are that they often produce large variance estimates, particularly for small areas with small sample sizes, and they do not produce the maps that users increasingly request.

Model-assisted estimators rely on both observations for population units selected for the sample and on predictions for population units not selected for the sample. However, because the validity of inference is still based on the probability sample, model-assisted estimators are characterized as probability-based. The model-assisted difference estimator (Baffetta et al., 2009; Särndal et al., 1992) can be expressed using information from an error matrix constructed using accuracy assessment data obtained from an equal probability sample (Table 1). The $n_{k,l}$ notation is commonly used with error matrices where n denotes a count, the first subscript denotes class observations, the second subscript denotes class predictions, and the $+$ subscript denotes all classes. Thus, $n_{F,F}$ denotes the number of pixels both observed and predicted to be forested (F), n_{F+} denotes the total number of pixels observed to be forested, and n_{+F} denotes the total number of pixels predicted to be forested. The difference estimator expresses the estimate of the population parameter, μ, as the mean of population unit predictions with a correction for the estimated bias,

$$\hat{\mu}_{Dif} = \frac{1}{N}\sum_{i=1}^{N}\hat{y}_i - \frac{n_{+F}-n_{F+}}{n}, \tag{4}$$

where $\hat{y}_i$ is the prediction for the ith population unit, and the subscript, *Dif*, denotes the model-assisted difference estimator (McRoberts, 2010). The variance of $\hat{\mu}_{Dif}$ is estimated as,

$$V\hat{a}r(\hat{\mu}_{Dif}) = \frac{1}{n(n-1)}\sum_{i=1}^{n}(\hat{y}_i-y_i)^2. \tag{5a}$$

Table 1
Error matrix.

		Predicted class		Total	Producer's accuracy
		F	NF		
Observed class	F	$n_{F,F}$	$n_{F,NF}$	n_{F+}	$\frac{n_{F,F}}{n_{F+}}$
	NF	$n_{NF,F}$	$n_{NF,NF}$	n_{NF+}	$\frac{n_{NF,NF}}{n_{NF+}}$
Total		n_{+F}	n_{+NF}	n	
User's accuracy		$\frac{n_{F,F}}{n_{+F}}$	$\frac{n_{NF,NF}}{n_{+NF}}$	OA $= \frac{n_{F,F}+n_{NF,NF}}{n}$	

Further, because y_i and $\hat{y}_i$ are both either 0 or 1,

$$(\hat{y}_i-y_i)^2 = \begin{cases} 0 & \text{for } \hat{y}_i=y_i, \text{ a correct prediction} \\ 1 & \text{for } \hat{y}_i\neq y_i, \text{ an incorrect prediction} \end{cases}.$$

Thus, $V\hat{a}r(\hat{\mu}_{Dif})$ can be expressed as,

$$\begin{aligned} V\hat{a}r(\hat{\mu}_{Dif}) &= \frac{n_{F,NF}+n_{NF,F}}{n(n-1)} \\ &= \frac{n_{+F}+n_{F+}-2n_{FF}}{n(n-1)} \end{aligned} \tag{5b}$$

(McRoberts, 2010). The model-assisted difference estimator is appropriate for use with any technique that produces a class prediction for each pixel, not just the logistic regression model approach.

3.3. Model-based inference

Model-based approaches to inference are based on the assumption of an entire distribution of possible observations for Y for each population unit, not just a single constant value as is the case for probability-based inference. Whereas randomization for probability-based inference enters through the random selection of population units into the sample, randomization for model-based inference enters through the randomness of observations from the distributions for individual population units. Thus, model-based approaches to inference do not necessarily require probability samples. Model-based approaches often focus on estimation of μ_i, the distribution expectation for each pixel which is a population parameter, rather than the particular observed land cover class which is a random realization from the distribution of possible classes. The variance of $\hat{\mu}_i$ is estimated as,

$$V\hat{a}r(\hat{\mu}_i) \approx Z_i' \hat{V}_{\hat{\beta}} Z_i,$$

where

$$z_{ij} = \frac{\partial f(X_i;\beta)}{\partial \beta_j},$$

and $\hat{V}_{\hat{\beta}}$ is the estimated parameter covariance matrix. The population mean is estimated as,

$$\hat{\mu}_{Mod} = \frac{1}{N}\sum_{i=1}^{N}\hat{\mu}_i, \tag{6}$$

where the subscript *Mod* denotes a model-based estimator. The variance of $\hat{\mu}_{Mod}$ is estimated as,

$$\begin{aligned} V\hat{a}r(\hat{\mu}_{Mod}) &= \frac{1}{N^2}\sum_{i=1}^{N}\sum_{j=1}^{N} C\hat{o}v\left(\hat{\mu}_i,\hat{\mu}_j\right) \\ &\approx \frac{1}{N^2}\sum_{i=1}^{N}\sum_{j=1}^{N} Z_i'\hat{V}_{\hat{\beta}}Z_j \end{aligned} \tag{7}$$

(McRoberts, 2006).

3.4. Simulating positional errors

For purposes of assessing the effects of positional errors on inferences for proportion forest area, the relationship between the FIA plot observations and the 12 spectral transformations as estimated using the logistic regression model was considered to be the true relationship, the estimated parameters were assumed to be the true parameters, and $p_i = f(X_i;\beta)$ was calculated for each pixel in each of the six 15-km × 15-km AOIs. A forest/non-forest observation for each

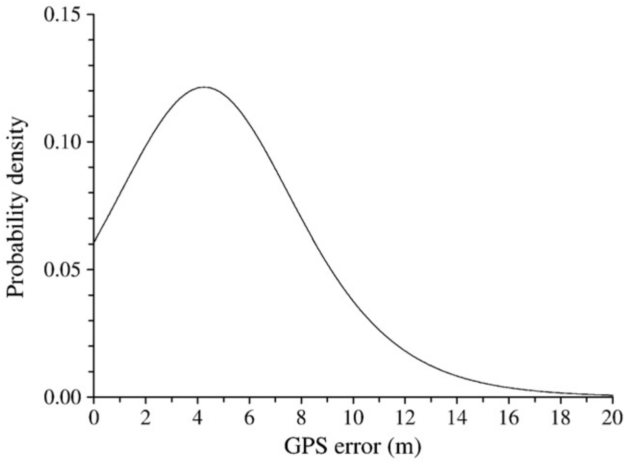

Fig. 2. Probability density function for GPS error.

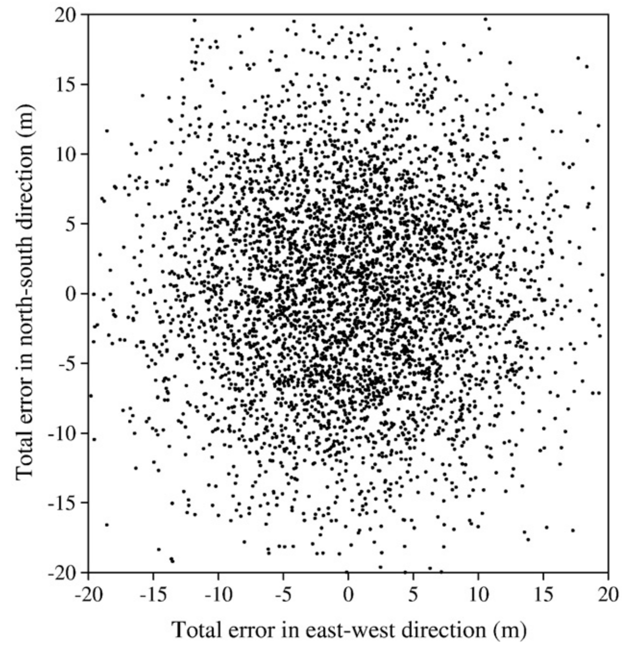

Fig. 3. Distribution of combined rectification and GPS errors where rectification error is from a Gaussian distribution with $\mu = 15$ m and $\sigma = 6$ m and the distribution of GPS errors is as depicted in Fig. 2.

pixel was simulated by drawing a random number, r, from a uniform (0,1) distribution and assigning non-forest ($y = 0$) to the pixel if $r < p_i$ and forest ($y = 1$) if $r \geq p_i$. The true proportion forest, μ_{Tru}, for each AOI and the aggregation of the six AOIs was calculated as the mean of the simulated values for all pixels. The GPS-based coordinates of the FIA central subplots and their assignments to pixels were assumed to be without error. Thus, the combination of the forest/non-forest assignments of the subplots and the spectral values of the pixels containing the subplot centers was assumed to constitute the sample. The logistic regression model was fit to these sample data, and $\hat{\mu}_{\mathrm{SRS}}$, $\hat{\mu}_{\mathrm{Dif}}$, and $\hat{\mu}_{\mathrm{Mod}}$, and their respective variance estimates were calculated for each AOI and the aggregation of the six AOIs. The estimates for individual AOIs are characterized as synthetic because they use information from outside the AOI; i.e., the logistic regression model was applied to individual AOIs although the model parameters were estimated using data for all six AOIs (Gonzalez, 1973).

The combined effects of image rectification and GPS errors on inferences for proportion forest area were assessed using a simulation procedure. First, image rectification errors were simulated by perturbing the coordinates of each subplot by randomly selecting an azimuth from a uniform $[0, 2\pi)$ distribution and a distance from a Gaussian distribution, $G(\mu,\sigma)$, with $\mu = 15$ m (TM half-pixel width) or $\mu = 30$ m (TM full pixel width) and $\sigma = 0.4\,\mu$. Distances greater than 2.5σ from μ were reselected which effectively limits the range of distances to [0 m, 30 m] or [0 m, 60 m]. Second, GPS errors were simulated by perturbing the coordinates of each subplot by randomly selecting an azimuth from a uniform $[0, 2\pi)$ distribution and a distance from a continuous distribution based on the histogram of GPS errors for FIA plots reported by Hoppus and Lister (2007) (Fig. 2). This distribution is consistent with the results reported by Jasumback (1996) in a test of GPS receivers. Image rectification and GPS errors were assumed to be independent, and were added to produce total positional errors (Fig. 3). The image pixels containing the perturbed subplot centers were then determined, the values of the spectral transformations were appended to the unchanged subplot forest/non-forest assignments, the logistic regression model was refit to the data, and $\hat{\mu}_{\mathrm{Dif}}$ and $\hat{\mu}_{\mathrm{Mod}}$, and their respective variance estimates were calculated. Because the subplot forest/non-forest observations do not change, $\hat{\mu}_{\mathrm{SRS}}$ and $\hat{\mathrm{Var}}(\hat{\mu}_{\mathrm{SRS}})$ do not change either. This procedure was repeated a large number of times for the two distributions of rectification errors both with and without GPS errors. For each of these four combinations, the proportion of subplots whose perturbed locations produced a change in pixel assignment was calculated. Also, for each of the four combinations and for each of the six 15-km × 15-km AOIs, the means over all simulations of $\hat{\mu}_{\mathrm{Dif}}$ and $\hat{\mu}_{\mathrm{Mod}}$, the means of their standard errors calculated as the square roots of their variance estimates, and overall accuracy (OA) as defined in Table 1 were calculated as were the proportions of two-standard error confidence intervals for each estimator, $\hat{\mu}_{\mathrm{Dif}}$ and $\hat{\mu}_{\mathrm{Mod}}$, that included the true forest area, μ_{Tru}.

4. Results and discussion

4.1. Comparison of estimators using sample data without positional errors

Differences between μ_{Tru} and the $\hat{\mu}_{\mathrm{SRS}}$ revealed the effects of small sample sizes, although all estimates were within two SRS standard errors of μ_{Tru} (Table 2). The model-assisted difference estimator and the model-based estimator produced estimates that were similar to μ_{Tru}, although only the model-based estimates were within two standard errors of μ_{Tru}. The failure of $\hat{\mu}_{\mathrm{Dif}}$ to produce estimates within two standard errors of μ_{Tru} is attributed to the nature of the variance estimator for the model-assisted approach. In particular, because the forest/non-forest class predictions were correct for all or a very high proportion of subplots, the standard error estimates, $\mathrm{SE}(\hat{\mu}_{\mathrm{Dif}})$, were either 0 or very small. Herein lies a difficulty with the model-assisted difference estimator for AOIs with small sample sizes; i.e., correct class predictions for all or a very high proportion of a small number of reference observations leads to estimates of 100% or very high accuracy for the classifications of all pixels in the AOI, a somewhat doubtful result.

Table 2
Estimates with no positional errors.

AOI	μ_{Tru}	n	$\hat{\mu}_{\mathrm{SRS}}$	$\mathrm{SE}(\hat{\mu}_{\mathrm{SRS}})$	$\hat{\mu}_{\mathrm{Dif}}$	$\mathrm{SE}(\hat{\mu}_{\mathrm{Dif}})$	$\hat{\mu}_{\mathrm{Mod}}$	$\mathrm{SE}(\hat{\mu}_{\mathrm{Mod}})$
1	0.774	14	0.667	0.126	0.740	0.000	0.740	0.061
2	0.606	15	0.357	0.133	0.602	0.000	0.602	0.022
3	0.924	16	0.938	0.063	0.880	0.000	0.880	0.041
4	0.945	16	0.875	0.085	0.905	0.000	0.905	0.035
5	0.665	14	0.714	0.125	0.621	0.105	0.621	0.067
6	0.843	16	0.688	0.120	0.794	0.000	0.794	0.046
All	0.793	91	0.714	0.048	0.757	0.016	0.757	0.048

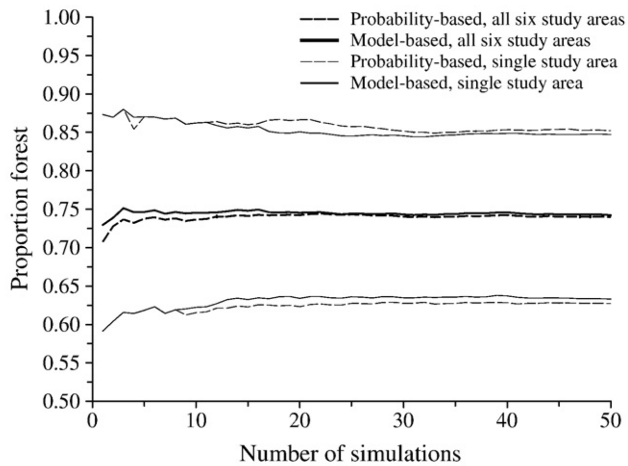

Fig. 4. Means over simulations versus number of simulations for estimates based on all six AOIs and two selected single AOIs.

4.2. Effects of positional errors on subplots

For each combination of the two rectification error distributions and exclusion or inclusion of GPS error, means of the estimates of $\hat{\mu}_{Dif}$ and $\hat{\mu}_{Mod}$ stabilized by 50 simulation replications for both individual AOIs and the aggregation of the six AOIs (Fig. 4). As the sum of the means of the rectification and GPS errors increased, the proportions of subplots that changed pixel assignments changed proportionately (Table 3). Over all AOIs, the proportions of subplots that changed pixel assignments ranged from 0.243 to 0.566. Of particular note, the proportions of subplots that changed pixel assignments for the rectification error distribution with mean 30 m, regardless of whether GPS errors were excluded or included, exceeded 0.50.

The proportions of subplots whose class predictions changed as a result of erroneous pixel assignments varied considerably by AOI, but over all AOIs ranged from 0.055 to 0.087. For the rectification error distribution with mean 30 m, inclusion of GPS errors had negligible additional detrimental effects. The greater detrimental effects of positional errors for more fragmented forests can be seen by comparing results for AOI 2 which had little fragmentation and AOI 5 which had considerable fragmentation (Table 4, Fig. 5).

4.3. Model-assisted difference estimator

The effects of increasing sums of rectification and GPS errors on model-assisted estimates were threefold. First, OA decreased as the magnitudes of errors increased; this finding has been well-documented by numerous others.

Second, the general effect of positional errors was to decrease $\hat{\mu}_{Dif}$ for both individual AOIs and the aggregation of all six AOIs (Table 4). The effects of positional errors were that some forested subplots were re-assigned to pixels whose spectral transformation values produce non-forest predictions and vice versa for non-forested plots. The result was that some subplots whose correct spectral transformation values produced $\hat{p} \geq 0.50$ from Eq. (1) were erroneously assigned to pixels whose spectral transformations produced smaller estimates of p; if $\hat{p}$ changed from $\hat{p} \geq 0.50$ to $\hat{p} < 0.50$, a change in class prediction resulted. Analogous results occurred for subplots whose correct spectral transformations produced $\hat{p} < 0.50$. In terms of proportions of subplots whose predictions changed from forest to non-forest or vice versa, the effects were greatest for $\hat{p}$ much less than 0.50, $\hat{p}$ much greater than 0.50, and for greater errors. The overall effect of this phenomenon was that as positional errors increased, model predictions, $\hat{p}$, for all population units shifted toward $\hat{\mu}_{SRS}$.

The third general effect was that proportions of two-standard error confidence intervals that included μ_{Tru} decreased as the magnitude of errors increased (Table 4). For the aggregation of the six AOIs, this result is attributed to two phenomena. First, as previously noted, errors of greater magnitude contributed to greater deviations between $\hat{\mu}_{Dif}$ and μ_{Tru}. Second, although the mean of SE($\hat{\mu}_{Dif}$) increased with errors of greater magnitude, the range of the distribution of SE($\hat{\mu}_{Dif}$) also increased with the result that some values of SE($\hat{\mu}_{Dif}$) were smaller than values obtained with no errors. The combination of deviations

Table 4
Means of estimates obtained with the model-assisted difference estimator.

Rectification error	GPS error	AOI	μ_{Tru}	$\hat{\mu}_{Dif}$	SE($\hat{\mu}_{Dif}$)	Cover[a]	OA
0	No	1	0.774	0.740	0.000		
		2	0.606	0.602	0.000		
		3	0.924	0.880	0.000		
		4	0.945	0.905	0.000		
		5	0.665	0.621	0.105		
		6	0.843	0.794	0.000		
		All	0.793	0.757	0.016		
15 m	No	1	0.774	0.749	0.021	0.26	0.98
		2	0.606	0.592	0.000	0.00	1.00
		3	0.924	0.852	0.020	0.22	0.98
		4	0.945	0.875	0.008	0.12	0.99
		5	0.665	0.627	0.103	1.00	0.86
		6	0.843	0.742	0.019	0.14	0.98
		All	0.793	0.740	0.019	0.30	0.97
15 m	Yes	1	0.774	0.713	0.051	0.54	0.94
		2	0.606	0.585	0.000	0.00	1.00
		3	0.924	0.871	0.035	0.44	0.96
		4	0.945	0.870	0.004	0.06	1.00
		5	0.665	0.615	0.105	1.00	0.86
		6	0.843	0.733	0.045	0.38	0.95
		All	0.793	0.731	0.023	0.24	0.95
30 m	No	1	0.774	0.673	0.078	0.70	0.89
		2	0.606	0.574	0.000	0.00	1.00
		3	0.924	0.840	0.035	0.38	0.96
		4	0.945	0.855	0.013	0.12	0.99
		5	0.665	0.585	0.106	1.00	0.85
		6	0.843	0.697	0.073	0.46	0.90
		All	0.793	0.704	0.027	0.12	0.93
30 m	Yes	1	0.774	0.685	0.070	0.64	0.90
		2	0.606	0.578	0.001	0.02	0.99
		3	0.924	0.849	0.048	0.48	0.95
		4	0.945	0.854	0.013	0.08	0.99
		5	0.665	0.595	0.106	0.96	0.85
		6	0.843	0.707	0.073	0.52	0.91
		All	0.793	0.711	0.027	0.12	0.93

[a] Proportion of two-standard error confidence intervals that included μ_{Tru}.

Table 3
Proportions of subplots changing pixel assignments and class predictions as a result of positional errors.

Mean rectification error	GPS error	Pixel assignment changes	Forest/non-forest prediction changes						
			AOI 1	AOI 2	AOI 3	AOI 4	AOI 5	AOI 6	All AOIs
15 m	No	0.243	0.092	0.000	0.018	0.039	0.017	0.031	0.055
15 m	Yes	0.321	0.117	0.000	0.025	0.032	0.153	0.059	0.063
30 m	No	0.509	0.173	0.000	0.038	0.047	0.137	0.121	0.086
30 m	Yes	0.566	0.179	0.003	0.044	0.036	0.164	0.101	0.087

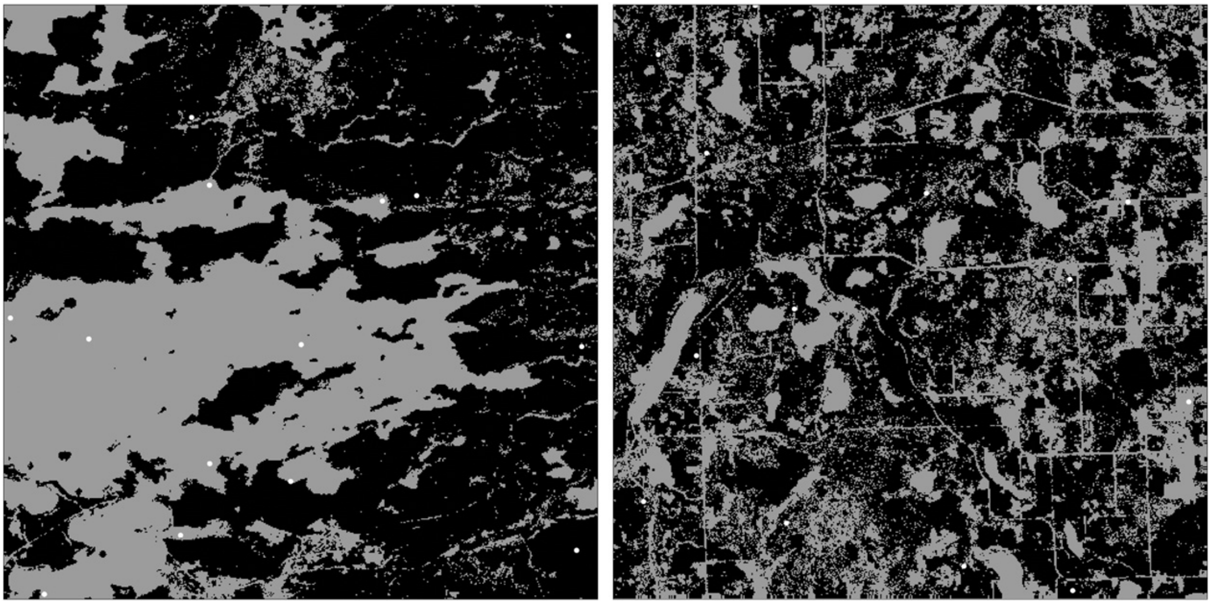

Fig. 5. AOIs 2 (left) and 5 (right) illustrating less and more forest fragmentation, respectively: black denotes forest, gray denotes non-forest, and white denotes plots.

between $\hat{\mu}_{\mathrm{Dif}}$ and μ_{Tru} and erroneously small SE($\hat{\mu}_{\mathrm{Dif}}$) produced disproportionately large numbers of confidence intervals that excluded μ_{Tru}.

For individual AOIs, the results for confidence intervals were highly variable, and only a few trends were discernible. One trend was that SE($\hat{\mu}_{\mathrm{Dif}}$) tended to increase as error magnitudes increased, although the results were highly dependent on individual AOIs. For example, because SE($\hat{\mu}_{\mathrm{Dif}}$) which is derived from Eqs. (5a) and (b) is based on differences between observations and predictions of forest/non-forest, SE($\hat{\mu}_{\mathrm{Dif}}$) for AOI 5 which had little fragmentation was not greatly affected by positional errors. A second trend was that OAs were quite large, even when positional errors were included.

4.4. Model-based estimator

The trend of increasing deviations between $\hat{\mu}_{\mathrm{Mod}}$ and μ_{Tru} with increasing errors was the same as for $\hat{\mu}_{\mathrm{Dif}}$ (Table 4). This trend was apparent for both individual AOIs and aggregations of the six AOIs.

The trend of decreasing proportions of two-standard error confidence intervals that included μ_{Tru} as the magnitude of errors increased was also the same for $\hat{\mu}_{\mathrm{Mod}}$ as for $\hat{\mu}_{\mathrm{Dif}}$ (Table 5). Although the means of SE($\hat{\mu}_{\mathrm{Mod}}$) obtained with positional errors were quite close to means obtained with no errors, the range of the distribution of SE($\hat{\mu}_{\mathrm{Mod}}$) obtained with positional errors increased with greater errors. The combination of increasing deviations between $\hat{\mu}_{\mathrm{Mod}}$ and μ_{Tru} and increasing proportions of small SE($\hat{\mu}_{\mathrm{Mod}}$) with increasing errors resulted in decreasing proportions of two-standard error confidence intervals that included μ_{Tru}. However, because SE($\hat{\mu}_{\mathrm{Mod}}$) was generally larger than SE($\hat{\mu}_{\mathrm{Dif}}$), even for individual AOIs, the coverage was more similar to what would be expected for two-standard error widths.

5. Conclusions

Two general and two specific conclusions may be drawn from the study. First, rectification and GPS errors obscure the true relationship between subplot observations spectral information and cause population unit estimates of proportion forest area to deviate toward $\hat{\mu}_{\mathrm{SRS}}$. These effects were similar for both the model-assisted difference estimator and the model-based estimator. Further, the effects were exacerbated for forested areas with greater fragmentation.

Second, the effects of rectification and GPS errors contributed to erroneously small coverages for two-standard error confidence intervals. This effect is attributed to deviations in estimates of proportion forest estimates and erroneously small variance estimates. The effect was more pronounced with the model-assisted difference estimator for which standard errors tended to be smaller than for the model-based estimator.

A specific conclusion is that the model-assisted difference estimator did not perform well for individual AOIs, although results

Table 5
Means of estimates obtained with the model-based estimator.

Rectification error	GPS error	AOI	μ_{Tru}	$\hat{\mu}_{\mathrm{Mod}}$	SE($\hat{\mu}_{\mathrm{Mod}}$)	Cover[a]
0	No	1	0.774	0.740	0.061	
		2	0.606	0.602	0.022	
		3	0.924	0.880	0.041	
		4	0.945	0.905	0.035	
		5	0.665	0.621	0.067	
		6	0.843	0.794	0.046	
		All	0.793	0.757	0.048	
15 m	No	1	0.774	0.740	0.059	1.00
		2	0.606	0.592	0.023	1.00
		3	0.924	0.847	0.043	0.74
		4	0.945	0.882	0.037	0.84
		5	0.665	0.633	0.061	1.00
		6	0.843	0.759	0.049	0.72
		All	0.793	0.742	0.048	1.00
15 m	Yes	1	0.774	0.719	0.059	0.92
		2	0.606	0.585	0.025	0.96
		3	0.924	0.842	0.043	0.68
		4	0.945	0.873	0.037	0.58
		5	0.665	0.616	0.060	0.92
		6	0.843	0.746	0.051	0.64
		All	0.793	0.730	0.048	0.94
30 m	No	1	0.774	0.688	0.062	0.88
		2	0.606	0.574	0.027	0.90
		3	0.924	0.840	0.047	0.68
		4	0.945	0.867	0.038	0.52
		5	0.665	0.590	0.060	0.84
		6	0.843	0.728	0.056	0.48
		All	0.793	0.714	0.050	0.82
30 m	Yes	1	0.774	0.700	0.059	0.84
		2	0.606	0.579	0.025	0.94
		3	0.924	0.845	0.044	0.70
		4	0.945	0.868	0.037	0.48
		5	0.665	0.601	0.057	0.86
		6	0.843	0.730	0.054	0.52
		All	0.793	0.720	0.048	0.80

[a] Proportion of two-standard error confidence intervals that included μ_{Tru}.

were acceptable for the aggregation of the six AOIs. This result is characteristic of probability-based estimators and can be attributed to small sample sizes for small AOIs.

Finally, a second specific conclusion is that for a distribution of rectification errors with mean of 30 m, equivalent to the width of one Landsat TM pixel, more than half the subplots were assigned to incorrect pixels. The potential adverse impacts of this finding on the ability to construct spatially accurate maps from medium or finer resolution imagery and to draw correct inferences from the maps are disconcerting. Of further concern, the prospects for constructing accurate maps when the forest class is divided into subclasses of finer thematic resolution such as coniferous and deciduous or forest type are even less optimistic.

These adverse effects of rectification and GPS errors indicate that investigation of methods for correcting or compensating for them warrants consideration.

References

Agresti, A. (2007). *An introduction to categorical data analysis*, 2nd edition New York: Wiley 372 pp.

Arbia, G., Griffith, D., & Haining, R. (1998). Error propagation modeling in raster GIS: Overlay operations. *Journal of Geographical Information Science*, *12*, 145−167.

Baffetta, F., Fattorini, L., Franceschi, S., & Corona, P. (2009). Design-based approach to *k*-nearest neighbours technique for coupling field and remotely sensed data in forest surveys. *Remote Sensing of Environment*, *11*, 463−475.

Barber, J. J., Gelfand, A. E., & Siiander, J. A., Jr. (2006). Modelling map positional error to infer true feature location. *Canadian Journal of Statistics*, *34*, 659−676.

The enhanced Forest Inventory and Analysis program — national sampling design and estimation procedures. Bechtold, W. A., & Patterson, P. L. (Eds.). (2005). *General Technical Report SRS-80. Southern Research Station, USDA Forest Service, Asheville, North Carolina* (85 pp. Available at: http://www.srs.fs.usda.gov/pubs/. Last accessed: July 2009).

Carmel, Y., Dean, D. J., & Flather, C. H. (2001). Combining location and classification error sources for estimating multi-temporal database accuracy. *Photogrammetric Engineering and Remote Sensing*, *67*, 865−872.

Cienciala, E., Tomppo, E., Snorrason, A., Broadmeadow, M., Colin, A., Dunger, K., et al. (2008). Preparing emission reporting systems from forests: Use of national forest inventories in European countries.*Silva Fennica*, *42*, 73−88 (Available at: http://www.metla.fi/silvafennica/sfquart.htm. Last accessed, June 2008).

Congalton, R. G. (2007). Thematic and positional accuracy assessment of digital remotely sensed data. In R. E. McRoberts, G. A. Reams, P. C. Van Deusen, & W. H. McWilliams (Eds.), *Proceedings of the Seventh Annual Forest Inventory and Analysis Symposium; 2005 October 3–6; Portland, ME. General Technical Report WO-77* (pp. 149−154). Washington, DC: U.S. Department of Agriculture Forest Service (Available at: http://www.fia.fs.fed.us/symposium/proceedings/. Last accessed July 2009).

Cooke, W. H. (2000). Forest/non-forest stratification in Georgia with Landsat Thematic Mapper data. In R. E. McRoberts, G. A. Reams, & P. C. Van Deusen (Eds.), *Proceedings of the First Annual Forest Inventory and Analysis Symposium. General Technical Report NC-213* (pp. 28−30). St. Paul, MN: U.S. Department of Agriculture, Forest Service, North Central Research Station (Available at: http://www.fia.fs.fed.us/symposium/proceedings/. Last accessed July 2009).

Crist, E. P., & Cicone, R. C. (1984). Application of the tasseled cap concept to simulated Thematic Mapper data. *Photogrammetric Engineering and Remote Sensing*, *50*, 343−352.

Czaplewski, R. L. (2005). Resampling remotely sensed data to improve national mapping of forest conditions. In M. Marsden, M. Downing, & M. Riffe (Eds.), *Workshop proceedings: Quantitative techniques for deriving national-scale data; Westminster, CO, July 26–28, 2005. FHTET-2005-12* (pp. 263−284). Fort Collins, CO: U.S. Dept. of Agriculture, Forest Service, Forest Health Technology Enterprise Team (Available at: http://www.fs.fed.us/foresthealth/technology/pub_titles.shtml. Last accessed: July 2009).

Dai, X., & Khorram, S. (1998). The effects of image misregistration on the accuracy of remotely sensed change detection. *IEEE Transactions on Geoscience and Remote Sensing*, *36*, 1566−1577.

Goodchild, M. F. (1994). Integrating GIS and remote sensing for vegetation analysis and modeling: Methodological issues. *Journal of Vegetation Science*, *5*, 615−626.

Gonzalez, M. E. (1973). Use and evaluation of synthetic estimates. *1973 Proceedings of the social statistics section, American Statistical Association* (pp. 33−36).

Halme, M., & Tomppo, E. (2001). Improving the accuracy of multisource forest inventory estimates by reducing plot location error — A multicriteria approach. *Remote Sensing of Environment*, *78*, 321−327.

Hansen, M. H., & Hahn, J. T. (1992). Determining stocking, forest type, and stand-size class from forest inventory data. *Northern Journal of Applied Forestry*, *9*, 82−89.

Hansen, M. H., Madow, W. G., & Tepping, B. J. (1978). An evaluation of model-dependent and probability-sampling inferences in sample surveys. *Journal of the American Statistical Association*, *78*, 776−793.

Hoppus, M., & Lister, A. (2007). The status of accurately locating Forest Inventory and Analysis plots using the global positioning system. In R. E. McRoberts, G. A. Reams, Paul C. Van Deusen, & W. H. McWilliams (Eds.), *Proceedings of the seventh annual forest inventory and analysis symposium; 2005 October 3–6; Portland, ME. General Technical Report WO-77* (pp. 179−184). Washington, DC: U.S. Department of Agriculture Forest Service Available at: http://www.fia.fs.fed.us/symposium/proceedings/. Last accessed July 2009.

Hoppus, M., Riemann, R., & Lister, A. (2001). Remote sensing strategies for Forest Inventory and Analysis utilizing the FIA plot database. In J. D. Greer (Ed.), *Proceedings of RS'2000, eighth biennial remote sensing applications conference: Remote sensing and geospatial technologies for the new millennium.* Albuquerque, NM: CD-ROM.

Jasumback, T. (1996). *GPS evaluation: West Coast test site.* Missoula, Montana: USDA Forest Service, Technology Development Center.

Kauth, R. J., & Thomas, G. S. (1976). The Tasseled Cap — A graphic description of the spectral–temporal development of agricultural crops as seen by Landsat. *Proceedings of the symposium on machine processing of remotely sensed data* (pp. 41−51). West Lafayette, IN: Purdue University.

Kendall, M. G., & Buckland, W. R. (1982). A dictionary of statistical terms, 4th edition . New York: Longman Group, Ltd.

Kyoto Protocol (1997). The Kyoto Protocol to the framework convention on climate change. Available at:. unfccc.int/essential_background/Kyoto_protocol/background/items/1351.php (Last accessed: July 2009).

Magnussen, S. (2007). A method for estimation of a land-cover change matrix from error-prone unit-level observations. *Canadian Journal of Forest Research*, *37*, 1505−1517.

McRoberts, R. E. (2006). A model-based approach to estimating forest area. *Remote Sensing of Environment*, *103*, 56−66.

McRoberts, R. E. (2010). Probability- and model-based approaches to inference for proportion forest using satellite imagery as ancillary data. *Remote Sensing of Environment*, *114*, 1017−1025.

McRoberts, R. E., Bechtold, W. A., Patterson, P. L., Scott, C. T., & Reams, G. A. (2005). The enhanced Forest Inventory and Analysis program of the USDA Forest Service: Historical perspective and announcement of statistical documentation. *Journal of Forestry*, *103*, 304−308.

McRoberts, R. E., Wendt, D. G., Nelson, M. D., & Hansen, M. H. (2002). Using a land cover classification based on satellite imagery to improve the precision of forest inventory area estimates. *Remote Sensing of Environment*, *81*, 36−44.

Ministerial Conference on the Protection of Forests in Europe (2009). Ministerial Conference on the Protection of Forests in Europe. Available at:. http://www.mcpfe.org/ (Last accessed: March 2009).

Montréal Process (2005). Montréal Process. Available at:. http://www.rinya.maff.go.jp/mpci/ (Last accessed: March 2009).

Patterson, P. L., & Williams, M. S. (2003). Effects of registration errors between remotely sensed and ground data on estimators of forest area. *Forest Science*, *49*, 110−118.

Pontius, G., Jr. (2000). Quantification error versus location error in comparison of categorical maps. *Photogrammetric Engineering and Remote Sensing*, *66*, 1011−1016.

Riemann, R., Hoppus, M., & Lister, A. (2000). Using arrays of small ground sample plots to assess the accuracy of Landsat TM-derived forest cover maps. In G. B. M. Heuvelink, & M. J. P. M. Lemmens (Eds.), *Proceedings of the 4th international symposium on spatial accuracy assessment in natural resources and environmental sciences* (pp. 541−548). Delft, The Netherlands: Delft University Press.

Rouse, J. W., Haas, R. H., Schell, J. A., & Deering, D. W. (1973). Monitoring vegetation systems in the Great Plains with ERTS. *Proceedings of the third ERTS symposium, NASA SP-351, volume 1* (pp. 309−317). Washington, DC: NASA.

Särndal, C. -E., Swensson, B., & Wretman, J. (1992). Model assisted survey sampling. New York: Springer-Verlag, Inc 694 pp.

Stow, D. A. (1999). Reducing the effects of misregistration on pixel-level change detection. *International Journal of Remote Sensing*, *12*, 2477−2483.

Tomppo, E., Gschwantner, T., Lawrence, M., & McRoberts, R. E. (2010). National forest inventories: Pathways to harmonized reporting. : Springer 612 pp.

Townshend, J. R. G., Justice, C. O., Gurney, C., & McManus, J. (1992). The impact of misregistration on change detection. *IEEE Transactions on Geoscience and Remote Sensing*, *30*, 1054−1060.

United Nations Framework Convention on Climate Change (UNFCCCC) (2007). National inventory submissions 2007. Available at:. http://unfccc.int/national_reports/items/1408.php (Last accessed: April 2009).